Received 11 August 2025; accepted 14 September 2025. Date of publication 22 September 2025; date of current version 2 October 2025.

Digital Object Identifier 10.1109/OJCOMS.2025.3612749

Optimized Resource Allocation for Delay-Tolerant ALOHA–NOMA for Enhancing the Performance of Underwater Acoustic Sensor Networks

VEERAPU GOUTHAM [1], (Member, IEEE), V. P. HARIGOVINDAN [2], (Senior Member, IEEE), MIRIYALA MAHESH [3], (Member, IEEE), AND DUSHANTHA NALIN K. JAYAKODY [4,5,6], (Senior Member, IEEE)

[1]Department of Communication Engineering, School of Electronics Engineering, Vellore Institute of Technology, Vellore 632014, India
[2]Department of Electronics and Communication Engineering, National Institute of Technology Puducherry, Karaikal 609609, India
[3]School of Electronics Engineering, VIT-AP University, Amaravati 522237, India
[4]COPELABS, Lusófona University, 1700-097 Lisboa, Portugal
[5]LASI, Centro de Tecnologia e Sistemas, UNINOVA, 2829-516 Costa da Caparica, Portugal
[6]CIET/DEEE, Faculty of Engineering, Sri Lanka Institute of Information Technology, Malabe 10115, Sri Lanka

CORRESPONDING AUTHOR: VEERAPU GOUTHAM (e-mail: gouthamveerapu@gmail.com)

This work was supported by the Vellore Institute of Technology (Vellore campus).

ABSTRACT In this work, we introduce a propagation delay-tolerant ALOHA–NOMA-based cross-layer protocol for enhancing the performance of Underwater Acoustic Sensor Networks (UASNs). Various phenomena such as multi-path fading, Doppler spread, frequency as well as distance-dependent path loss, and limited available distance-dependent bandwidth have a significant impact on performance of UASNs. Due to these distinct characteristics, ALOHA is often considered a viable medium access control (MAC) protocol for UASNs, even though ALOHA is inefficient as far as channel utilization is concerned. Recently, non-orthogonal multiple access (NOMA) has been envisioned as a thriving enabling technology to meet the burgeoning demands of energy-constrained and bandwidth-constrained UASNs. As a result, we propose propagation delay-tolerant ALOHA-NOMA, where NOMA is employed in the physical layer with optimal utilization of distance-dependent bandwidth and transmission power, to improve the performance of ALOHA-based UASNs. We derive closed-form expressions for the MAC layer utilization factor, goodput, and energy consumption in UASNs by taking into account UASN channel characteristics. Results show that the proposed ALOHA-NOMA scheme significantly improves the performance of UASNs. Finally, we also derive mathematical expressions for the optimal channel attempt rate to maximize the MAC layer utilization factor. The analytical results are validated through extensive ns-3 simulations.

INDEX TERMS ALOHA-NOMA, energy consumed per bit, goodput, MAC layer utilization factor, non-orthogonal multiple access, underwater acoustic sensor networks, underwater ALOHA, Internet of Underwater Things.

I. INTRODUCTION

THE OCEAN, covering more than 70% of the Earth's surface, plays a vital role in sustaining life. It regulates global climate, influences weather patterns, and provides essential resources for human societies. Additionally, it serves as a key avenue for international trade and transportation. Despite its immense significance, more than 95% of the ocean remains unexplored and uncharted. This underscores the need to carry out ocean exploration and environmental protection in a conscious, long-term, and appropriate manner. In recent decades, underwater networking technologies have gained considerable attention due to their broad range of applications, including natural disaster monitoring, tactical surveillance, underwater medical research, and ocean exploration [1], [2], [3]. With the growing number of these applications, it is foreseeable that the

widespread deployment of underwater devices, facilitating the expansion of the Internet of Underwater Things (IoUT) on a larger scale [4], [5], [6]. The realization of cost-efficient underwater sensor networks that can support diverse communication requirements contributes to the expansion of the Internet of Things into the oceanic realm, often referred to as IoUT [7]. Underwater wireless networks predominantly use radio, optical, and acoustic technologies, each used for specific requirements. Radio communication utilizes electromagnetic waves, but their effectiveness is limited to short distances due to high absorption losses in conductive seawater. Optical communication, which employs light waves for data transfer, is similarly constrained to short-range applications due to line-of-sight requirements and signal scattering caused by particles in the water. Acoustic communication, which relies on sound waves, is often preferred over radio and optical communication technologies due to its relatively lower absorption losses, and enabling successful long-distance underwater wireless communication. However, the underwater acoustic medium presents lot of challenges, including long propagation delays, low data transmission rates, and high bit error rates. Besides the higher propagation delays, frequency-dependent and distance-dependent signal attenuation further impact energy consumption, making power requirements heavily reliant on both transmission distance and available bandwidth.

Underwater acoustic sensor networks (UASNs) also face significant energy constraints due to the limited battery capacity of wireless sensor nodes. Recharging or replacing these batteries is often impractical. Moreover, a substantial portion of node's energy consumption is associated with signal transmission and reception. In UASNs, the energy required for data packet transmission rises with increasing transmission distance. Elevated energy consumption leads to faster depletion of a node's power resources, ultimately reducing the lifetime of the network. Therefore, optimizing energy consumption per bit is a key consideration in the design of communication protocols for UASNs. Given the unique characteristics of the underwater communication channel, a comprehensive system-level approach is essential to achieve minimal energy consumption per bit, enhanced data transmission rates among underwater nodes, and the interconnection of myriads of underwater devices (larger connectivity).

In recent years, extensive research has focused on underwater medium access control (MAC) protocols [2], [8], [9], [10], [11], [12], [13], [14], [15], [16]. To reduce and prevent data packet collisions, it is essential to implement a control mechanism for efficiently allocating underwater channel resources. Here, the fundamental objective of MAC protocols is to minimize collisions while maintaining energy efficiency, reducing channel access delays, and ensuring network fairness. Essentially, MAC protocols govern how nodes share channel resources. Similar to terrestrial wireless sensor networks (WSNs), MAC protocols play a crucial role in UASNs and significantly impact overall network performance. However, UASN MAC layers encounter substantial challenges due to long propagation delays, low data transmission rates, and the limited bandwidth of acoustic communication [14], [17], [18], [19], [20], [21], [22], [23]. Traditional multiple access techniques such as TDMA, FDMA, and CDMA are generally inefficient for low-duty-cycle traffic networks. Moreover, the long propagation delays in UASNs further complicate MAC layer design by limiting the effectiveness of centralized access control and time-slotting methods [13], [14], [24]. Additionally, carrier sensing becomes highly expensive due to these propagation delays. Consequently, distributed random access protocols like ALOHA are considered the most feasible MAC layer solutions for UASNs [2], [14]. ALOHA is one of the earliest multiple access protocols initially designed for terrestrial WSNs [25]. In its original form, pure ALOHA allowed nodes to transmit data immediately whenever they needed to send information. Later, the concept of slotted ALOHA variant was introduced, segmenting the transmission time into discrete slots. In this scheme, nodes are only allowed to transmit at the beginning of each time slot, thereby reducing the probability of packet collisions. Given its simplicity and the inherent challenges of acoustic communication, such as significant propagation delays—ALOHA remains one of the most extensively studied MAC protocols for underwater networks. The study in [11] analyzed the effect of spatio-temporal uncertainty on UASNs and concluded that slotted ALOHA does not offer significant advantages over pure ALOHA in such networks. In [12], an analytical framework was presented to assess the performance of both pure and slotted ALOHA protocols in UASNs, revealing that propagation delay has minimal impact on the performance of pure ALOHA in single-hop UASNs. Furthermore, several studies [9], [14], [21], [26] have explored cross-layer design strategies aimed at enhancing throughput, reducing energy consumption, and prolonging network lifetime in UASNs.

Non-orthogonal multiple access (NOMA) has emerged as a promising technology for addressing the growing demands (especially in achievable channel rates) of next-generation UASNs. Generally, NOMA can be implemented by utilizing either the power or code domains [27], [28], [29], [30], [31], [32], [33], [34]. The fundamental concept behind NOMA is to exploit the power or code domain to facilitate multiple simultaneous transmissions within a single resource block. In power-domain NOMA, the source node transmits multiple users' information by allocating different power levels to each user within a single resource block, which may be defined in terms of time, frequency, or code domain. The key techniques enabling NOMA include superposition coding and successive interference cancellation (SIC) [35]. In this work, our main focus is on up-link data transmission using NOMA, where multiple users non-orthogonally transmit their signals in the power-domain to the autonomous underwater vehicle (AUV) within an orthogonal resource block. The AUV employs SIC to decode the transmitted signals by first extracting the stronger user's

signal and then removing it from the composite signal to decode the weaker user's information. A major challenge in uplink NOMA is ensuring a sufficient disparity in received signal power levels from different nodes, allowing the SIC receiver at the AUV to decode them accurately. To address this, fractional power control (FPC) has been adopted in terrestrial wireless uplink NOMA, ensuring differentiated reception of signal strengths at the base station. Given the bandwidth limitations in UASNs, NOMA presents a viable approach for enhancing data rates without any requirement of the additional bandwidth. Several studies have explored the application of NOMA in underwater wireless communication to improve system throughput. The works in [36], [37], [38], [39], [40] examined potential of NOMA for increasing the sum rate in underwater networks. Additionally, the studies in [40], [41] proposed a method for boosting underwater channel data rates by incorporating full-duplex cooperative relay techniques with NOMA.

By considering the simplicity of ALOHA alongside the superior spectral efficiency of NOMA and its capability to resolve collisions through SIC receivers [42], this research introduces ALOHA-NOMA as a promising MAC protocol for bandwidth-limited and energy-constrained UASNs. The integration of ALOHA with NOMA helps to mitigate ALOHA's inherent limitations, such as low throughput efficiency, high collision rates, and reduced energy efficiency. Many existing ALOHA-based UASN studies primarily focus on MAC layer analysis without considering essential physical layer properties of the underwater channel, such as distance-dependent transmission power and bandwidth variations with distance. In this research, we adopt a cross-layer modeling approach for ALOHA-NOMA, specifically designed for bandwidth-constrained and energy-limited UASNs. The proposed scheme incorporates ALOHA at the MAC layer and NOMA at the physical layer, enabling a more efficient allocation of network resources. It is important to note that the ALOHA-NOMA scheme also provides a practical solution for avoiding scheduling by allowing increased number of UASN devices to transmit to the AUV within a single resource slot. Many previous studies [14], [15] assume equidistant transmitters and receivers, which is often unrealistic in ad-hoc UASN environments, where the distances between source and destination nodes vary. In this work, we consider a network where source and destination nodes are uniformly distributed within a circular region. Furthermore, the proposed scheme enhances energy efficiency by eliminating the need for UASN devices to sense the channel before transmission, thereby reducing power consumption while maintaining robust communication performance.

The key contributions of this paper are outlined as follows:

1) We propose an ALOHA-based non-orthogonal multiple access (ALOHA-NOMA) MAC protocol for bandwidth-limited and energy-constrained underwater acoustic sensor networks (UASNs), wherein NOMA is employed at the physical layer and ALOHA is utilized for channel access at the MAC layer.
2) We derive closed-form analytical expressions for key performance metrics, including the MAC layer utilization, goodput, and energy efficiency, while incorporating underwater-specific factors such as distance-dependent bandwidth, acoustic spreading, and multipath fading. Furthermore, we present an analytical derivation of the optimal attempt rate that maximizes MAC layer utilization.
3) We present an optimal resource allocation framework based on a hybrid deep deterministic policy gradient (DDPG) and pattern search approach to jointly optimize distance-dependent bandwidth allocation and transmission power, thereby enhancing the performance of ALOHA-NOMA-based UASNs.
4) We validate the proposed framework through extensive simulations, demonstrating substantial performance improvements over conventional UASN protocols in terms of MAC layer utilization, goodput, and energy efficiency.

TABLE 1. List of acronyms.

AL	Absorption Losses
AUV	Autonomous Underwater Vehicle
DI	Directivity Index
FPC	Fractional Power Control
IoT	Internet of Things
IoUT	Internet of Underwater Things
MAC	Medium Access Control
NOMA	Orthogonal Multiple Access
NL	Ambient Noise Level
PHY layer	Physical Layer
SIC	Successive Interference Cancellation
SL	Source Level
SNR	Signal-to-Noise Ratio
TL	Transmission Losses
UASN	Underwater Acoustic Sensor Network
WSN	Wireless Sensor Network

To the best of our knowledge, this study is the first to evaluate the performance of ALOHA-NOMA for UASNs. The remainder of the paper is structured as follows: Section II presents the UASN model along with the proposed ALOHA-NOMA scheme and derives expressions for the probability of success and energy efficiency. Section II-B.5 focuses on optimizing MAC layer utilization with respect to the attempt rate. Section III provides numerical and simulation results, while Section V concludes the paper. The list of acronyms and symbols used in this work are given in Table 1 and 2, respectively.

II. UNDERWATER ALOHA-NOMA

This section covers: (1) the physical layer modeling of underwater acoustic networks, (2) the proposed ALOHA-NOMA scheme for UASNs, and (3) the mathematical modeling along with the derivation of precise expressions for

TABLE 2. List of symbols.

Γ	Signal-to-noise ratio
r	Transmission distance in km
f	Signal frequency
η	Geometric spreading factor
A	Anomalies in transmission loss
$\alpha(\varsigma, \Theta, f)$	The absorption coefficient (in dB/km)
Θ	Temperature
ς	Depth
ν_1	Relaxation frequencies (in kHz) for boric acid
ν_2	Relaxation frequencies (in kHz) for magnesium sulphate
Λ_i and ζ_i	Arbitrary coefficients
χ	Salinity
κ	Sound speed in seawater
$S(f)$	Transmitted signal's power spectral density
B_r	Distance dependent available bandwidth
P_{tr}	Transmit power
B	Bandwidth coefficient
P	Power coefficient
Q and T	Positive constants
S_i	Source node from region i
$f_d(d)$	Probability density function
T_{wi}	The waiting time for source node in region i
t_r	Start time of the next available time slot
T_{pi}	Propagation delay for the region i
h_i	Fading channel coefficient
P_m	The probability that m nodes attempt to access a channel
P_i	The probability of an idle time slot
P_s	Probability of a successful transmission
P_c	Probability of collision
λ	Attempt rate
$U()$	MAC layer uitilization factor
$G()$	Goodput
E	Energy consumed per bit

the probability of success and energy efficiency of ALOHA-NOMA in UASNs.

A. PHYSICAL LAYER MODEL

In this subsection, we outline the physical layer model used for computing the signal-to-noise ratio (SNR) in underwater acoustic networks [43], [44]. The signal-to-noise ratio (Γ) at the receiver in UASNs is described using the passive sonar equation as follows:

$$\Gamma_{in\ dB} = SL - TL - (NL - DI), \tag{1}$$

where SL denotes the source level, TL represents the transmission loss, NL is the ambient noise level, and DI refers to the directivity index. TL comprises both spreading and absorption losses. According to [45], the total TL experienced between communicating nodes in an underwater acoustic environment is expressed as:

$$TL(r,f) = \eta \times 10\log r + r \times 10^{-3} \times 10\log\alpha(\varsigma, \Theta, f) + A, \tag{2}$$

where η indicates the geometric spreading factor, r is the distance in kilometers, A accounts for anomalies in transmission loss, and $\alpha(\varsigma, \Theta, f)$ denotes the absorption coefficient (in dB/km), which varies with frequency f (in kHz), temperature Θ, and depth ς. The absorption model used here is valid within the range 100 Hz $< f <$ 1 MHz, and is defined as [46], [47]:

$$\alpha(\varsigma, \Theta, f) = \frac{\Lambda_1\zeta_1\nu_1 f^2}{f^2+\nu_1^2} + \frac{\Lambda_2\zeta_2\nu_2 f^2}{f^2+\nu_2^2} + \Lambda_3\zeta_3 f^2, \tag{3}$$

where f is the operating frequency. The terms ν_1 and ν_2 represent the relaxation frequencies (in kHz) for boric acid and magnesium sulphate, respectively. The coefficients Λ_i and ζ_i (for $i \in \{1,2,3\}$) capture dependencies on temperature, salinity, and depth on acoustic signal absorption. The mathematical expressions for finding these coefficients are given by,

$$\begin{aligned}
\nu_1 &= 2.8\left(\frac{\chi}{35}\right)^{0.5} 10^{\left[4-\frac{1245}{273+\Theta}\right]} \\
\nu_2 &= \frac{8.17\times 10^{\left[8-\frac{1990}{273+\Theta}\right]}}{1+18\times 10^{-4}(\chi-35)} \\
\Lambda_1 &= \frac{8.68}{\kappa} \times 10^{(0.78\ pH-5)} \\
\Lambda_2 &= 21.44(1+0.025\,\Theta)\frac{\chi}{\kappa} \\
\Lambda_3 &= \begin{cases} 4.937\times 10^{-4} - 2.59\times 10^{-5}\Theta + 9.11\times 10^{-7}\Theta^2 \\ \quad +9.11\times 10^{-7}\Theta^2 - 1.50\times 10^{-8}\Theta^3 \quad \text{for } \Theta \le 20^\circ C \\ 3.964\times 10^{-4} - 1.146\times 10^{-5}\Theta + 1.45\times 10^{-7}\Theta^2 \\ \quad -6.5\times 10^{-10}\Theta^3 \quad \text{for } \Theta > 20^\circ C \end{cases} \\
\zeta_1 &= 1 \\
\zeta_2 &= 1 - 1.37\times 10^{-4}\varsigma + 6.2\times 10^{-9}\varsigma^2 \\
\zeta_3 &= 1 - 3.83\times 10^{-5}\varsigma + 4.9\times 10^{-10}\varsigma^2,
\end{aligned} \tag{4}$$

where χ is the salinity and κ is the sound speed in seawater. The sound speed in sea is mainly affected by temperature, sea depth and salinity of sea water, and is given by [43], [48],

$$\begin{aligned}
\kappa = {} & 1448.96 + 4.591\Theta - 0.05304\Theta^2 + 0.0002374\Theta^3 + \\
& 1.340(\chi-35) + 0.0163\varsigma + 1.675\times 10^{-7}\varsigma^2 \\
& - 0.01025\Theta(\chi-35) - 7.139\times 10^{-13}\Theta\varsigma^3.
\end{aligned} \tag{5}$$

Ambient noise in underwater channels is primarily composed of four sources: turbulence ($N_t(f)$), shipping ($N_s(f)$), wave action ($N_w(f)$), and thermal effects ($N_{th}(f)$). Their power spectral densities (in dB re 1μPa per Hz) are described using empirical models:

$$\begin{aligned}
10\log_{10} N_t(f) &= 17 - 30\log_{10} f, \quad \text{for } f < 10 \text{ Hz} \\
10\log_{10} N_s(f) &= \begin{cases} 40 + 20(s-0.5) + 26\log_{10} f \\ -60\log_{10}(f+0.03), \\ \quad \text{for } 10 < f < 100 \text{ Hz} \end{cases} \\
10\log_{10} N_w(f) &= \begin{cases} 50 + 7.5w^{0.5} + 20\log_{10} f \\ -40\log_{10}(f+0.4), \\ \quad \text{for } 0.1 \text{ kHz} < f < 100 \text{ kHz} \end{cases} \\
10\log_{10} N_{th}(f) &= -15 + 20\log_{10} f, \quad \text{for } f > 100 \text{ kHz},
\end{aligned} \tag{6}$$

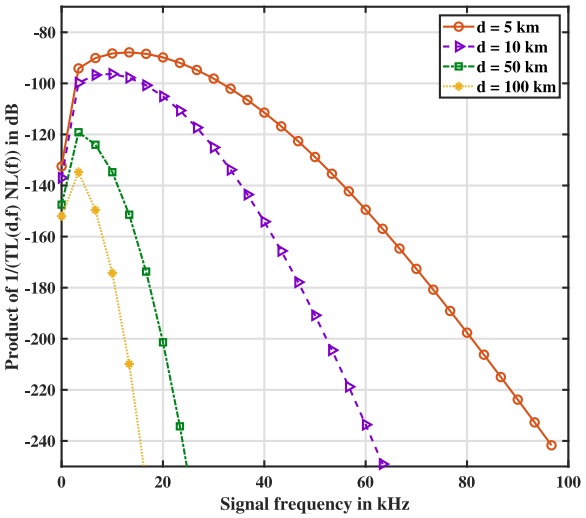

FIGURE 1. Product of $\frac{1}{TL(r,f)NL(f)}$ vs signal frequency.

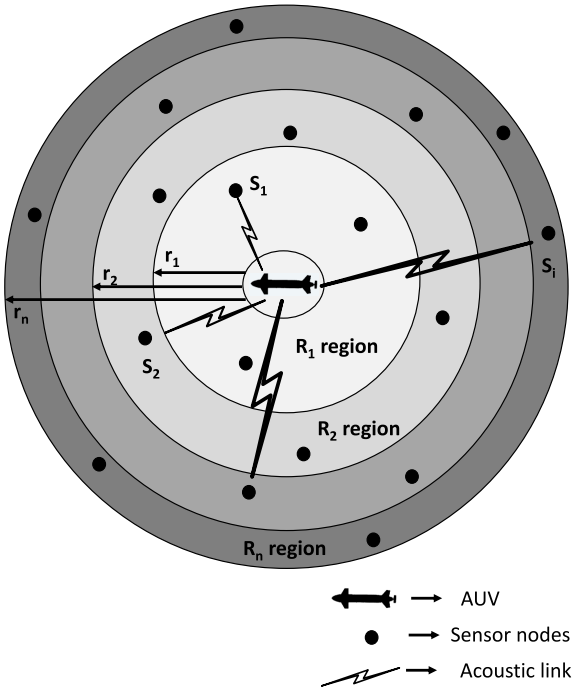

FIGURE 2. Underwater ALOHA-NOMA for UASNs.

where w represents wind speed, and s reflects shipping activity. Typically, higher frequencies result in lower noise levels. The total ambient noise p.s.d., denoted as $NL(f)$, is the summation of all four noise components. An approximate expression for $NL(f)$ is given by: $10\log_{10}(NL(f)) = 50 - 18\log_{10}(f)$ [49]. The product of $\frac{1}{TL(r,f)NL(f)}$ vs signal frequency is depicted in Fig. 1. It is evident from the Fig. 1 that as the transmission distance increases, the negative peak value of this product shifts toward lower frequencies. This indicates that higher-frequency signals experience significantly greater attenuation and noise over longer distances, making them less likely to reach the receiver effectively. Consequently, we can infer that shorter transmission distances support a broader usable bandwidth, including higher frequencies. In contrast, longer distances constrain the effective bandwidth to lower-frequency components due to increased pathloss and noise at higher frequencies. Therefore, the available bandwidth is inversely related to transmission distance—nodes at shorter distances benefit from higher available bandwidth, while nodes at longer distances are limited to lower-bandwidth channels. The SNR $\Gamma(r,f)$ between two transceiving nodes is defined as [49]:

$$\Gamma(r,f) = \frac{\frac{S(f)\Delta f}{AL(r,f)}}{NL(f)\Delta f} = \frac{S(f)}{TL(r,f)NL(f)}, \tag{7}$$

Here, $S(f)$ refers to the transmitted signal's power spectral density, which equals SL for frequencies $f \in B_r$, and zero elsewhere. The function B_r represents the bandwidth that varies with distance. As a result, total transmitted power is $P_{tr} = SL \cdot B_r$. From [49], [50], it follows that $B_r = Br^{-Q}$ and $P_{tr} = Pr^{T}$, where B and P are the bandwidth and power coefficients, and Q and T are positive constants. In UASNs, both transmission loss and noise are functions of signal frequency and node separation. Hence, the achievable ergodic capacity under frequency-dependent noise conditions is expressed as:

$$\begin{aligned} C &= E\left[\int_{f_l}^{f_u} \log_2(1+\Gamma(r,f))\ df\right], \\ &= E\left[\int_{f_l}^{f_u} \log_2\left(1+\frac{P_{tr}}{B_r TL(r,f)NL(f)}\right)\ df\right], \end{aligned} \tag{8}$$

where $E[\ \cdot\ ]$ indicates expectation, $f_l = f$, and $f_u = f + B_r$.

B. UNDERWATER ALOHA-NOMA FOR UASNS

We consider a single-hop UASN network consisting of $N-1$ source nodes and one sink node/ autonomous underwater vehicle (AUV). Because the UASN is ad-hoc network, the distances between the destination and source nodes are not always equal. As a result, we assume a network made up of one AUV and $N-1$ source nodes spread across the two-dimensional disc area with radius R as shown in Fig. 2. The AUV is located at the disc's center, and the source nodes are deployed uniformly throughout the disc area. Without loss of generality of up-link transmission, we consider all the source nodes transmit the sensed information to the AUV located at the center of a disc as shown in Fig. 2. For successful implementation of up-link NOMA transmission, we consider the total signal reception area of an AUV is divided into r different regions, *i.e.*, $R_i, i \in [1, r]$ based on the distance as shown in Fig. 2. The distance between a source node and AUV is denoted by d. As a result, the probability density function of d is given by, $f_d(d) = \frac{2d}{R^2}, d \in (0, R)$. Among all the source nodes associated with the AUV,

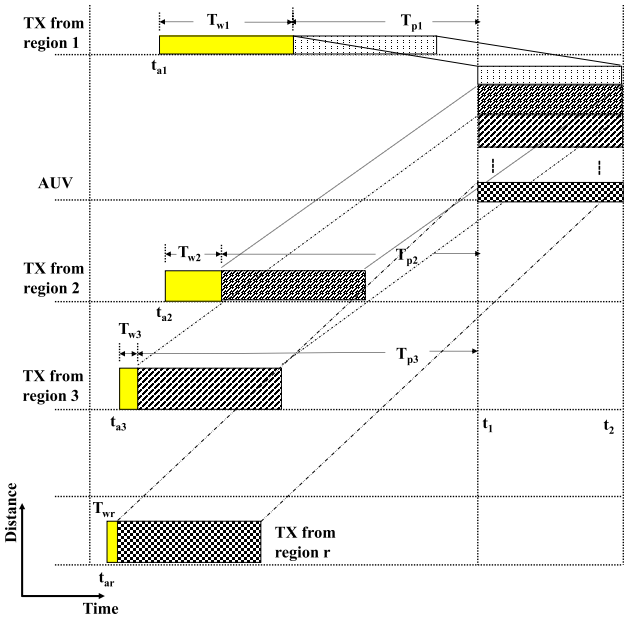

FIGURE 3. Timing diagram of data packet synchronization at the AUV of ALOHA-NOMA based UASNs.

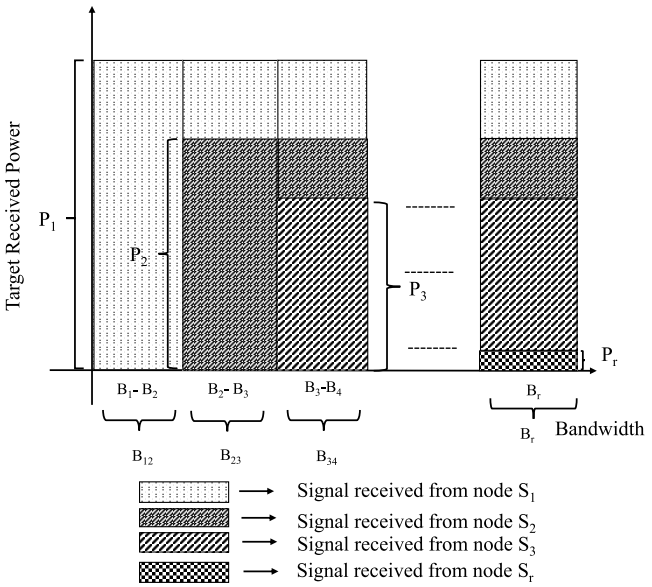

FIGURE 4. Power allocation scheme for ALOHA-NOMA.

only one distinct node from each region is selected for uplink NOMA transmission as shown in Fig. 2. Accordingly, a sensor node denoted by S_1 transmits the data packet from region R_1, and whose distance to AUV is d_1, $d_1 \in (0, r_1)$. S_2 node is selected from the region R_2 to transmit the data packet, and whose distance to AUV is d_2, which is greater than r_1 and less than r_2, $d_2 \in (r_1, r_2)$. Similarly, S_i node is selected from the region R_i to transmit the data packet, whose distance to AUV is d_i, which is greater than r_{i-1} and less than r_i, $d_i \in (r_{i-1}, r_i)$. Denoting the distance between S_i node and AUV as d_i, the pdf of d_1 is $f_{d_1}(d_1) = \frac{2d_1}{r_1^2}, d_1 \in (0, r_1)$, the pdf of d_2 is $f_{d_2}(d_2) = \frac{2d_2}{r_2^2 - r_1^2}, d_2 \in (r_2, r_1)$, and the pdf of d_i is $f_{d_i}(d_i) = \frac{2d_i}{r_i^2 - r_{i-1}^2}, d_i \in (r_i, r_{i-1})$.

1) DATA PACKET SYNCHRONIZATION AT THE AUV OF ALOHA-NOMA BASED UASNs

Unlike terrestrial wireless networks, UASNs experience performance variations due to their sensitivity to fluctuations in propagation delay. The speed of sound in seawater is primarily affected by temperature, depth, and salinity [43], [48]. Due to these uncertainties in propagation speed, achieving precise synchronization of data packets at the receiver is challenging, even when the exact distance between the source node and the AUV is known. In our proposed scheme, synchronization is possible if the source nodes are aware of their distance to the AUV and wait for an appropriate duration before transmitting a frame, as illustrated in Fig. 3.

The waiting time for source node S_1 in region R_1, denoted as T_{w1}, is expressed as: $T_{w1} = t_r - (t_{a1} + T_{p1})$ where t_r represents the start time of the next available time slot following $(t_{a1} + T_{p1})$, t_{a1} is the frame arrival time at source node S_1, and T_{p1} denotes the propagation delay from S_1 to the AUV. Similarly, for a source node S_i located in region R_i, the waiting time T_{wi} is given by: $T_{wi} = t_r - (t_{ai} + T_{pi})$ where t_{ai} represents the frame arrival time at source node S_i, and T_{pi} denotes the propagation delay from S_i to the AUV.

In the case of time-synchronized reception, illustrated in Fig. 3, the condition $t_r = t_1$ holds. This ensures that data packets arrive precisely within a designated time slot, where the slot size matches the data packet transmission time. Consequently, all transmitted packets reach the AUV within the same time slot but at varying power levels.

2) POWER ALLOCATION SCHEME FOR ALOHA-NOMA BASED UASNS

We assume that the channel link between the AUV and the tagged source node $S_i, i \in [1, r]$ follows an independent and identically distributed Rayleigh fading model, represented by the fading coefficient $h_i, i \in [1, r]$. The channel gain from S_i to the AUV can be expressed as $h_i \times TL(r_i, f)^{-1}$, where $h_i, i \in [1, r]$ are independent Rayleigh fading coefficients due to the multi-path propagation characteristics of UASNs. Consequently, the channel powers $|h_i|^2, i \in [1, r]$ are exponentially distributed random variables with the probability density function given by $f_Z(z) = \beta' e^{-\beta' z}$ for $z \geq 0$, where β' represents the average channel power. In UASNs, nodes from different regions have different available bandwidths and required transmission power levels [49]. As per [49], the available bandwidth and required transmission power levels are given by $B_r = Br^{-Q}$ and $P_{tr} = Pr^T$, respectively. It has been observed that the required transmission power level increases with increase in the transmission distance, whereas the available bandwidth decreases with increase in the transmission distance. Based on these observations,

we propose a novel power allocation scheme for ALOHA-NOMA, considering both available bandwidth and required transmission power levels, as illustrated in Fig. 4.

Generally, a source node closer to the AUV has greater available bandwidth than nodes farther away. In Fig. 4, B_1, B_2, ..., B_r denote the average available bandwidths for the regions R_1, R_2, $\cdots$, R_r, respectively. It follows that $B_1 > B_2 > \ldots > B_r$ and $\bigcap_{i=1}^{r} B_i = B_r$. Similarly, a source node closer to the AUV has a higher target received power level compared to nodes farther away. Source nodes from middle regions have higher target received power levels at the AUV than the nodes from far regions, and lower target received power levels at the AUV than the nodes closer to the AUV. Thus, the required transmission power increases with distance. We consider P_{t1}, P_{t2}, ..., P_{tr} as the average required transmission power levels for regions R_1, R_2, ..., R_r, respectively, satisfying $P_{t1} < P_{t2} < \cdots < P_{tr}$. As a result, the source node (S_i) computes the available bandwidth (B_i) and required transmission power levels (P_{ti}) based on the distance (d_i) from AUV to source node (S_i). Due to varying path losses in different regions, the proposed power allocation scheme ensures that signals are received at different power levels at the AUV, enabling successful symbol decoding using a successive interference cancellation (SIC) at the receiver. The respective received power levels for nodes from regions R_1, R_2, ..., R_r at the AUV are denoted as P_1, P_2, ..., P_r, as shown in Fig. 4. A source node in region i, $i \in [1, r]$, transmits data with power P_{ti}, $i \in [1, r]$ using the available bandwidth B_i, $i \in [1, r]$. We define $B_{12} = B_1 - B_2$, $B_{23} = B_2 - B_3$, and $B_r = B_r$. As illustrated in Fig. 4, the bandwidth B_{12} is exclusively available to node S_1 due to the near region node to the AUV, while B_{23} is available to both S_1 and S_2. Similarly, bandwidth B_r is accessible to all nodes associated with the AUV. Consequently, data packets from all r regions are received at the AUV within the B_r bandwidth, whereas in B_{ii+1}, packets from the first i regions are received at the AUV. In B_{12}, only packets from region 1 are received at the AUV. Thus, the AUV employs different SIC receivers across different bandwidths.

Based on the (8), the data rate achieved by node S_1 in the B_{12} bandwidth is given by,

$$C_{11} = E\left[\int_{B_{12}} \log_2\left(1 + \frac{|h_1|^2\rho_1}{B_{12}}\right) df\right]. \tag{9}$$

where $\rho_1 = \frac{P_{t1}}{TL(r_1,f)NL(f)}$.

The data rates achieved by nodes S_1 and S_2 within the B_{23} bandwidth are given by,

$$C_{21} = E\left[\int_{B_{23}} \log_2\left(1 + \frac{\frac{|h_1|^2\rho_1}{B_{23}}}{1 + \frac{|h_2|^2\rho_2}{B_{23}}}\right) df\right], \tag{10}$$

$$C_{22} = E\left[\int_{B_{23}} \log_2\left(1 + \frac{\frac{|h_2|^2\rho_2}{B_{23}}}{1 + \frac{\epsilon|h_1|^2\rho_1}{B_{23}}}\right) df\right]. \tag{11}$$

where $\rho_2 = \frac{P_{t2}}{TL(r_2,f)NL(f)}$, and ϵ varies in the range [0, 1], with $\epsilon = 0$ representing perfect SIC, while other values indicate imperfect SIC (I-SIC), i.e., interference from residual signals. As a result, the data rates achieved by nodes S_j in the B_{ii+1} bandwidth is given by,

$$C_{ij} = E\left[\int_{B_{ii+1}} \log_2\left(1 + \frac{\frac{|h_j|^2\rho_j}{B_{ii+1}}}{1 + \sum_{\substack{k=1,\\ j\geq 2}}^{j-1} \frac{\epsilon|h_k|^2\rho_k}{B_{ii+1}} + \sum_{\substack{k=j+1,\\ j+1\leq i}}^{i} \frac{|h_k|^2\rho_k}{B_{ii+1}}}\right) df\right], \tag{12}$$

where $i \geq j$, $\rho_j = \frac{P_{tj}}{TL(r_j,f)NL(f)}$. *Theorem 1:* For $i \geq j$, $j \geq 2$, and $j + 1 \leq i$, the analytical expression for the average data rate achieved by node S_j within the B_{ii+1} bandwidth is expressed as,

$$C_{ij} = \int_{B_{ii+1}} \left(\prod_{m=1}^{i} \beta_m\right)\left(\sum_{n=1}^{i} \frac{1}{B_{ii+1}}(\ln(B_{ii+1}) - e^{(\beta_n B_{ii+1})} Ei(-B_{ii+1}\beta_n)\right)\right) df$$

Proof: See Appendix A. ■

3) CALCULATION OF MAC LAYER UTILIZATION AND GOODPUT

The source nodes transmit the sensed data to the AUV under the assumption that all nodes are saturated, meaning they continuously have data packets to send. We assume that all source nodes follow an independent and identically distributed Poisson process with a uniform attempt rate of λ. In case of a packet collision, the source nodes retransmit their packets in the next available transmission time slot. This study focuses on the uplink NOMA transmission from source nodes to the AUV, representing a scenario where source nodes report sensing information to the AUV, as illustrated in Fig. 2. The sensor nodes utilize ALOHA as the MAC layer protocol while employing NOMA at the physical layer. Let P_s denote the probability of a successful data packet transmission from a source node to the AUV, and let T represent the packet transmission time. The probability that m nodes attempt to access a channel within a given time slot is given by,

$$P_m = \frac{((N-1)\lambda T)^m e^{-((N-1)\lambda T)}}{m!}. \tag{13}$$

The probability of an idle time slot, where no nodes attempt to access the channel, is expressed as,

$$P_i = e^{-((N-1)\lambda T)}. \tag{14}$$

Theorem 2: The probability of a successful transmission is defined as the scenario where no more than r nodes transmit simultaneously, ensuring that only one node from each region is transmitting in a given time slot. If multiple nodes from the same region transmit at the same time, is considered as collision in the this work. Therefore, the probability of a successful transmission is given by,

$$P_s = \sum_{j=1}^{r} \binom{r}{j} \frac{\left(\frac{N}{r}\right)^j}{\binom{N}{j}} \frac{((N-1)\lambda T)^j e^{-((N-1)\lambda T)}}{j!}, \tag{15}$$

where $\binom{r}{j}\frac{\left(\frac{N}{r}\right)^j}{\binom{N}{j}}$ accounts for the number of ways in which at most one node transmits from each region.

Proof: See Appendix B. Consequently, the probability of collision is given by,

$$P_c = 1 - P_i - P_s. \tag{16}$$

The MAC layer utilization factor can be expressed as,

$$U(\lambda) = \frac{T}{T + \frac{1}{\lambda}} \sum_{j=1}^{r} \binom{r}{j} \frac{\left(\binom{\frac{N}{r}}{1}\right)^j}{\binom{N}{j}} \frac{((N-1)\lambda T)^j e^{-((N-1)\lambda T)}}{j!}, \tag{17}$$

which measures the efficiency of MAC layer resource utilization. Finally, the goodput of a node is given by,

$$G(C, \lambda) = C \times U(\lambda), \tag{18}$$

where $C = \sum_{i=1}^{r} \sum_{j=1}^{i} C_{ij}$ represents the total achievable PHY layer data rate in the ALOHA-NOMA framework. ■

4) CALCULATION OF ENERGY CONSUMPTION PER BIT

The energy consumption per bit of a node can be modeled as follows: During each transmission, a node spends an energy amount of P_{avg}. Between consecutive transmissions, the node remains in a sleep state for a duration of $\frac{1}{\lambda}$. As a result, the energy consumed during the sleep period is given by $\frac{P_{\text{sleep}}}{\lambda}$.

Theorem 3: The probability of successful transmission is given by P_s, which results in the following expression for the energy consumed per bit:

$$E = \sum_{j=1}^{r} \frac{P_{tj} + \frac{P_{sleep}}{\lambda}}{P_{s_j} \times C_j} \tag{19}$$

where C_j represents the average data rate.

Proof: See Appendix C. ■

5) MAXIMIZATION OF MAC LAYER UTILIZATION

In this subsection, we present the maximization of MAC layer utilization factor of ALOHA-NOMA with respect to attempt rate in IoUT networks. Here, we derive analytical expressions for the channel attempt rate (λ^*) that maximizes the MAC layer utilization $U(\lambda)$. $U(\lambda)$ is maximized at the following channel access rate. It is obtained by differentiating (17) with respect to λ and equating to zero, *i.e.*, $\frac{dU(\lambda)}{d\lambda}|_{\lambda^*} = 0$,

Theorem 4:

$$\frac{dU(\lambda)}{d\lambda} = \frac{d}{d\lambda}\left(\frac{T}{T + \frac{1}{\lambda}} \sum_{j=1}^{r} \binom{r}{j} \frac{\left(\binom{\frac{N}{r}}{1}\right)^j}{\binom{N}{j}} \frac{((N-1)\lambda T)^j e^{-((N-1)\lambda T)}}{(j)!}\right) \tag{20}$$

we consider $a = (N-1)T$. The characteristic equation is given by,

$$\sum_{j=1}^{r}\left[\frac{T}{(\lambda T+1)^2} + \frac{\lambda T}{(\lambda T+1)}\left[\frac{j}{\lambda} - a\right]\right]\binom{r}{j}\frac{\left(\binom{\frac{N}{r}}{1}\right)^j}{\binom{N}{j}} \frac{(a\lambda)^j e^{-(a\lambda)}}{(j)!} = 0 \tag{21}$$

Proof: See Appendix D. Here, we consider conventional aloha protocol as case-1, in which only one source node transmitting the data packet in a particular resource time slot for successful transmission. As a result, no region splitting required for the implementation of conventional ALOHA protocol. Accordingly,

Case-1: ALOHA ($r = 1,\ j = 1$)

The characteristic equation and attempt rate that maximizes the MAC layer utilization factor in case-1 are given by,

$$aT\lambda^2 + (a - T)\lambda - 2 = 0, \tag{22}$$

$$\lambda^* = \frac{\sqrt{(a+T)^2 + 4aT} - (a - T)}{2aT}. \tag{23}$$

Whereas in case-2, we consider ALOHA-NOMA protocol in which two or less than two nodes are transmitting the data packet in a particular resource time slot for successful transmission. Accordingly, we divide the total signal reception area of an AUV into two different regions by considering $r = 2$.

Case-2: ALOHA-NOMA ($r = 2,\ j = 1, 2$)

The characteristic equation of case-2 is given by,

$$v_1\lambda^3 + v_2\lambda^2 + v_3\lambda - v_4 = 0 \tag{24}$$

where $v_1 = a^2NT$, $v_2 = 2NT^2 - aT(N+4)$, $v_3 = T(4 + 3N) - 4a$, and $v_4 = 8$. Finally, case-3 considers ALOHA-NOMA protocol in which three or less than three nodes are transmitting the data packet in a particular resource slot for successful transmission. Hence, we divide the total signal reception area of an AUV into three different regions by setting $r = 3$.

Case-3: ALOHA-NOMA ($r = 3,\ j = 1, 2, 3$)

The characteristic equation of case-2 is given by,

$$v_5\lambda^4 - v_6\lambda^3 - v_7\lambda^2 - v_8\lambda - 2 = 0 \tag{25}$$

where $v_5 = aTv_9$, $v_6 = [(3T - a)v_9 - av_{10}]$, $v_7 = 4v_9 + (2T - a)v_{10} - aT$, $v_8 = 3v_{10} - a + T$, and $v_9 = \frac{Na^2}{27(N-1)(N-2)}$, and $v_{10} = \frac{Na}{3(N-1)}$. Deriving the exact roots for higher order non-linear equations is tedious to solve. As a result, we use MATLAB 2018b software to find the roots for the characteristic equations of case-2 and case-3, after the substituting the numerical values of all the parameters involved in the characteristic equation. ■

III. RESULTS AND DISCUSSIONS

This section presents both analytical (Ana.) and simulation-based (Sim.) results to assess the performance of the

TABLE 3. Parameters.

Parameters	Values
Bandwidth coefficient (B)	19.76 $dB\ re\ \mu kHz$
Bandwidth exponent (Q)	0.59 $dB\ re\ \frac{kHz}{km}$
Power coefficient (P)	127.25 $dB\ re\ \mu Pa$
Power exponent (T)	2.07 $dB\ re\ \frac{\mu Pa}{km}$
Salinity (χ)	30 parts per thousand
Depth in Km	0.1 Km for shallow water
Depth in Km	3 Km for deep water
Wind speed (w)	6.67 m/s (average wind speed)
Shipping activity (s)	0.5 (average value)
Operating frequency range	1 kHz to 170 KHz
Directivity index (DI)	0 dB for omni-directional
ϵ	0.001
Noise model	ns3::UanNoiseModelDefault
Propagation model	ns3::UanPropModelThorp
Transmit mode	ns3::UanTxMode
MAC Layer	ns3::UanMacAloha
mobility model	ns3::ConstantPositionMobilityModel

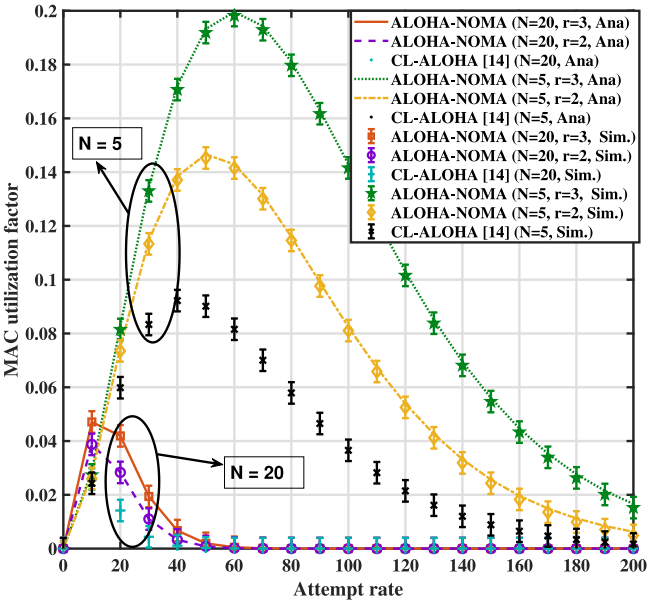

FIGURE 5. MAC utilization factor vs attempt rate.

TABLE 4. Maximization of MAC layer utilization with respect to attempt rate.

Scheme	Value (λ^*, N =20)	Value (λ^*, , N =5)
ALOHA	10.04585	42.5390
ALOHA-NOMA (r=2)	11.93193	51.29111
ALOHA-NOMA (r=3)	13.43105	59.93491

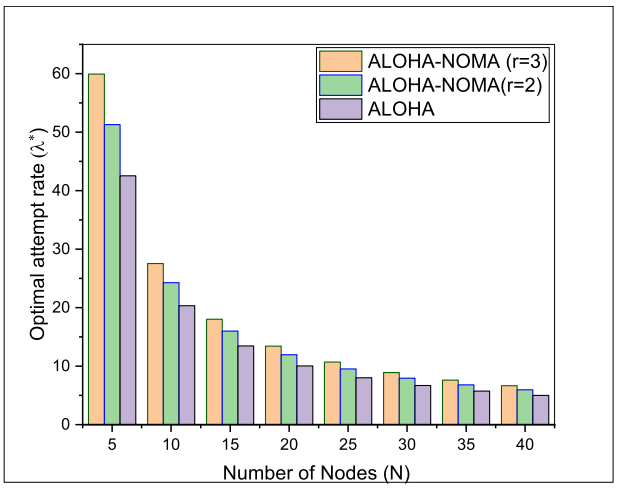

FIGURE 6. Optimal attempt rate (λ^*) vs Number of Nodes.

ALOHA-NOMA scheme. The ns-3 UAN module is utilized to simulate the underwater acoustic channel, which accurately models both attenuation losses and ambient noise, as these factors are strongly frequency-dependent. For the simulations, the acoustic channel model uses the Thorp attenuation model to compute the signal-to-noise ratio (SNR) at the receiver, considering the effects of ambient noise. The time slot duration T is set to 2 seconds, and the total simulation duration is 20,000 seconds. The network consists of N nodes, each located at different depths and uniformly distributed around the AUV, which is situated at the center of the coverage area. A comparative performance evaluation is conducted between the proposed ALOHA-NOMA scheme and the conventional ALOHA approach, with a focus on key performance indicators such as MAC layer utilization, goodput, and energy consumption per bit. For this analysis, two different configurations of the proposed scheme are considered, where the total signal reception area of the AUV is divided into two regions ($r = 2$) and three regions ($r = 3$). The parameters used in the performance evaluation are summarized in Table 3. Figure 5 shows a comparative analysis of ALOHA-NOMA and conventional ALOHA in terms of MAC Layer utilization factor with respect to the attempt rate for two cases of the number of nodes: 5 and 20. The results indicate that the MAC layer utilization factor improves as the number of region splitting in the AUV signal reception area increases. This increase in region splitting allows for a greater number of nodes to effectively utilize the MAC layer resources. Through the integration of NOMA and ALOHA, the AUV can decode data packets using a Successive Interference Cancellation (SIC) receiver even when more than one node transmits data packets simultaneously. Table 4 presents the values of the attempt rate at which the MAC layer utilization factor reaches its maximum. The positive root of the characteristic equation, denoted as λ^*, represents the attempt rate at which this maximum occurs. These values were determined using MATLAB 2018b software, after inputting all the necessary numerical values into the characteristic equation. It is evident from Table 4 that the attempt rate (λ^*) increases with a greater number of region splitting.

Figure 6 illustrates the relationship between the optimal attempt rate and the number of nodes present in the AUV signal reception area. It is evident from Fig. 6 that as

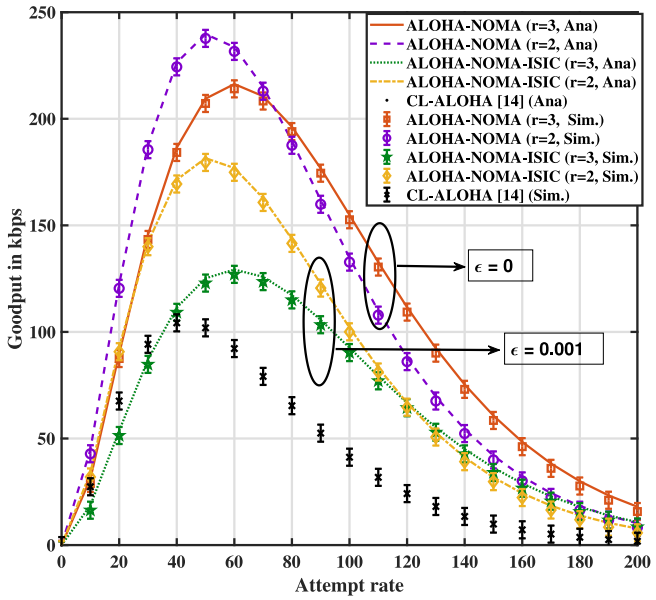

FIGURE 7. Goodput vs attempt rate.

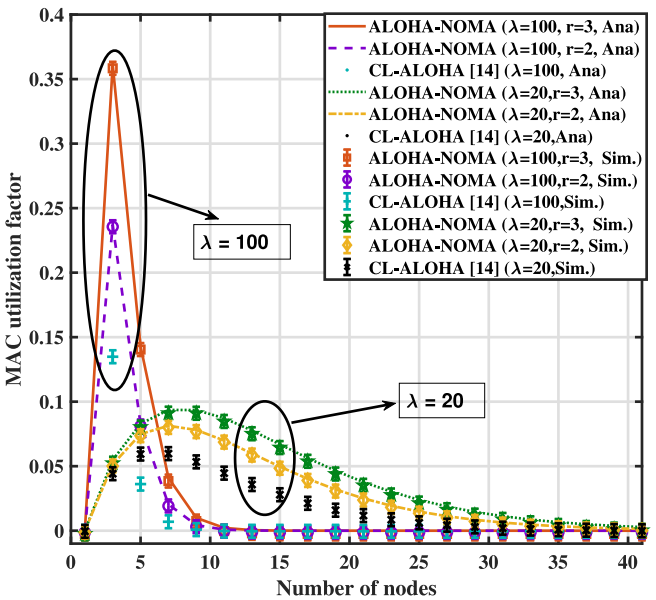

FIGURE 8. MAC utilization vs number of nodes.

the number of nodes in the AUV signal reception area increases, there is a corresponding increase in collision rates. Consequently, this increase in the number of nodes leads to a decrease in the optimal attempt rate, resulting in a reduction in collision rates.

In Fig. 7, we present a comparative analysis of ALOHA-NOMA and conventional ALOHA in terms of goodput with respect to the attempt rate. Goodput is primarily influenced by two factors: the achievable data rate at the PHY layer and the MAC layer utilization factor. As the number of regions splitting in the AUV signal reception area increases, the MAC layer utilization factor also increases. However, in the case of ALOHA-NOMA, there is an interesting observation when comparing the scenarios where number of regions (r) equal 2 and 3. The PHY layer achievable data rate in the r $=$ 2 scenario is higher than that in the r $=$ 3 scenario. This difference arises because the overall signal interference increases as the number of simultaneous transmissions in a particular resource time slot increases. Consequently, there is a crossover point in the goodput of ALOHA-NOMA between the r $=$ 2 and r $=$ 3 cases. Thus, up to a certain threshold attempt rate, the goodput of ALOHA-NOMA in the r $=$ 2 scenario outperforms other schemes. Beyond this threshold attempt rate, the goodput of ALOHA-NOMA in the r $=$ 3 scenario surpasses other schemes, owing to its superior MAC layer utilization factor in this scenario.Furthermore, it's worth noting that ALOHA-NOMA consistently achieves superior goodput compared to conventional ALOHA in both the r $=$ 2 and r $=$ 3 scenarios.

Figure 8 shows the variation of the MAC layer utilization factor with respect to the number of nodes for two different attempt rates, specifically for $\lambda = 100$ and $\lambda = 20$. From Fig. 8, it is clear that the MAC layer utilization factor initially increases and then decreases as the number of nodes in the network grows. This trend is mainly due to the increasing likelihood of collisions as more nodes are added, leading to a reduction in MAC layer utilization. In contrast, the proposed scheme demonstrates a increase in MAC layer utilization when the number of nodes increases at the start. This improvement is attributed to the NOMA technique, which allows multiple users to transmit data simultaneously using superposition coding. As a result, the proposed scheme outperforms the conventional ALOHA approach when the number of nodes is large. For networks with a low number of nodes, a higher attempt rate contributes to increased MAC layer utilization. Figure 9 depicts the average energy consumption per bit, expressed in $\frac{\mu \text{ Pa}\times\text{s}}{\text{bit}}$, as a function of the attempt rate. The average energy consumption per bit follows an inverse relationship with the variation of MAC layer utilization as a function of the attempt rate. From Fig. 9, it is evident that the lowest average energy consumption per bit is achieved in the $r = 2$ scenario compared to the other configurations. This is because the $r = 2$ scenario can achieve higher data rates while consuming less power than the $r = 3$ scenario.

IV. HYBRID DDPG WITH PATTERN SEARCH OPTIMIZATION

We adopt a hybrid optimization strategy that combines Deep Deterministic Policy Gradient (DDPG), a model-free deep reinforcement learning method with Pattern Search, a classical derivative-free local search algorithm. DDPG is especially suited for high-dimensional continuous action spaces and learns a deterministic policy by approximating both the Q-function and the policy network. However, DDPG can suffer from convergence to suboptimal policies due to function approximation errors and sparse reward structures. To overcome these limitations, we integrate Pattern Search into the DDPG learning loop to locally

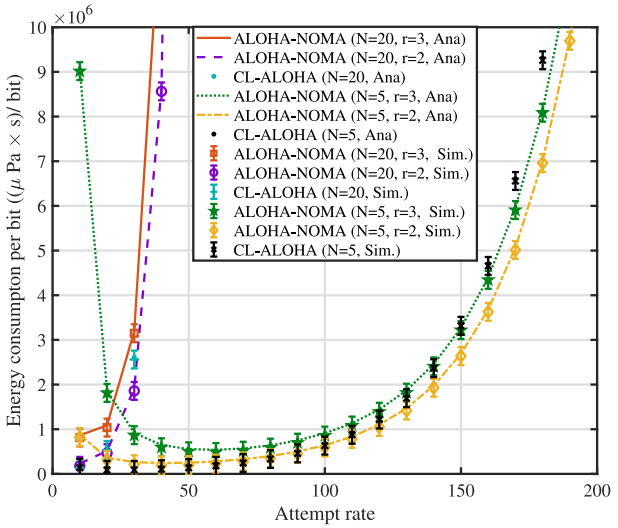

FIGURE 9. Energy consumption per bit ($\frac{\mu\ \text{Pa}\times\text{s}}{\text{bit}}$) vs attempt rate.

refine the actions proposed by the DDPG agent as shown in Fig. 10. This hybrid DDPG-PS algorithm improves the convergence rate and quality of solutions, especially in non-differentiable environments like ours, where computing gradients analytically or even numerically is impractical. While this approach does not yield symbolic expressions for optimal power and bandwidth allocations, it enables efficient numerical discovery of near-optimal policies. In our model, we aim to optimize the transmit powers, bandwidth allocations, and packet arrival rate to minimize the energy per successfully transmitted bit in a ALOHA-NOMA based UASNs. The devices are divided into r regions, each assigned different bandwidths and power levels. The optimization variables are: noitemsep

- $P_{t1}, P_{t12}, P_{t3}, \ldots, P_{tr}$: Transmit powers for Region 1 to Region r
- $B_{12}, B_{23}, B_{43}, \ldots, B_r$: Bandwidths allocated for Region 1 to Region r
- λ: Channel attempt rate

The energy efficiency objective function is given by:

$$E_{min} = \sum_{j=1}^{r} \frac{P_{tj} + \frac{P_{sleep}}{\lambda}}{P_{s_j} \times C_j} \tag{26}$$

where $\bar{P}$ is the average acoustic transmit power, C_{total} is the total achievable channel rate from both regions, and S_{12}, S_{22} are the access probabilities derived from Poisson traffic models. Subject to the constraints:

$$0 \leq P_{t1}, P_{t12}, P_{t3}, \ldots, P_{tr} \leq P_{\max}$$
$$0 \leq B_{12}, B_{23}, B_{43}, \ldots, B_r \leq P_{\max}$$
$$0 < \lambda < \lambda_{\max}$$

A. DDPG-PATTERN SEARCH RESULT

Figure 11 illustrates the learning curve of the hybrid DDPG with pattern search algorithm during training. The x-axis represents the number of training episodes, while the y-axis denotes the average episodic reward, which correlates inversely with energy consumption (since the objective is to minimize energy per successfully transmitted bit). Initially, the DDPG agent explores a wide range of policies with lower rewards due to random exploration. Periodically, the pattern search module is activated to locally refine the policy outputs, allowing the algorithm to escape poor local optima and stabilize around high-performing regions.

The result table presents the optimized values of transmit power, bandwidth allocations, packet arrival rates, and the resulting energy efficiency metric E_{min} for various network configurations. As the number of regions increases from 1 to 3, a significant improvement in energy efficiency

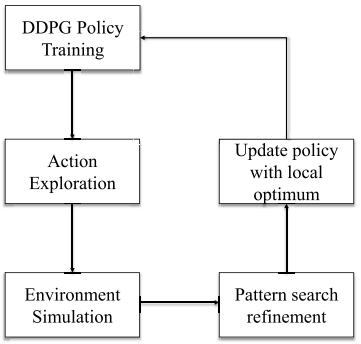

FIGURE 10. Hybrid DDPG + Pattern Search Optimization Loop.

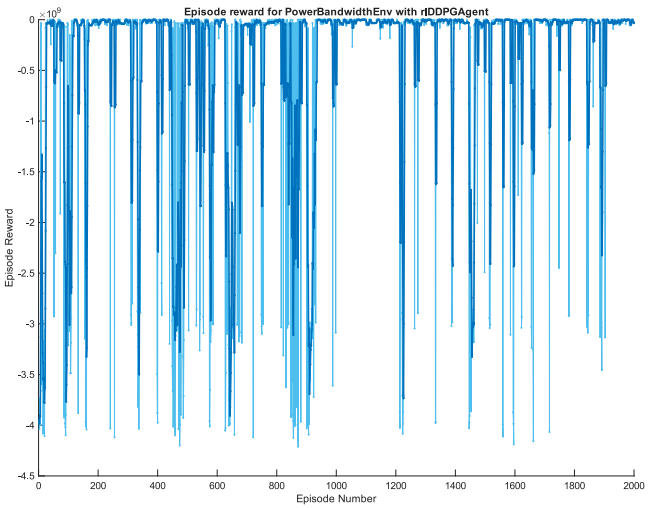

FIGURE 11. Hybrid DDPG Training.

TABLE 5. Hybrid DDPG-pattern search optimum results.

Number of nodes	Number of regions	P_{t1}	P_{t2}	P_{t3}	B_{12}	B_{23}	B_3	(λ)	E_{Min}
10	1	106497	-	-	0.89	-	-	9	9.5900e+04
25	1	245249	-	-	0.89	-	-	5	9.4343e+04
50	1	68545947	-	-	0.89	-	-	2	9.3233e+04
10	2	1537	33025	-	0.05	0.2	-	17	1.1455e+03
25	2	910209	3136	-	0.02	0.9	-	7	2.2204e+03
50	2	997809	1911		0.02	0.89	-	3	2.4080e+03
10	3	508384	495776	491616	0.101	0.101	0.89	25	1.0902e+01
25	3	505376	498848	510750	0.10	0.10	0.87	10	1.3098e+01
50	3	982304	8480	448	0.10	0.10	0.87	5	1.4352e+00

is observed, demonstrating the advantage of region-wise resource allocation. For example, with 50 nodes and a single region, the energy consumption remains high ($E_{min} = 9.3233e + 4$), whereas dividing the network into three regions reduces the energy metric to 1.4352, highlighting the effectiveness of spatial reuse and localized control. The hybrid DDPG-pattern search algorithm successfully adapts the transmit power and bandwidth according to node density and region count, while dynamically tuning the attempt rate λ to achieve a balance between transmission reliability and energy expenditure.

V. CONCLUSION

In conclusion, within the context of UASNs, distributed random access MAC protocols, such as ALOHA, have historically been considered as a practical choice. However, the primary limitation of ALOHA is the suboptimal utilization of MAC layer resources. To address this limitation, we propose a cross-layer design approach based on ALOHA-NOMA for UASNs, mainly focused on improving MAC layer resource utilization, goodput, and energy efficiency. In our proposed approach, MAC layer utilizes ALOHA, while NOMA is implemented at the physical layer. Our results demonstrate a significant improvement in several key performance metrics, including MAC layer utilization, goodput, and energy consumption per bit, compared to traditional ALOHA-based methods. Additionally, we have derived analytical expressions for the channel attempt rate that maximizes the MAC layer utilization factor. These results collectively highlight the effectiveness of our cross-layer design in optimizing UASN performance, paving the way for improved resource utilization and overall network efficiency.

APPENDIX A
DERIVATION OF THEOREM 1

Proof: After simplification, the data rates achieved by nodes S_j in the B_{i1+1} bandwidth is given by,

$$C_{ij} = E\left[\int_{B_{ii+1}} \log_2\left[\frac{B_{ii+1} + \sum_{k=1}^{j-1}\epsilon|h_k|^2\rho_k + \sum_{k=j}^{i}|h_k|^2\rho_k}{B_{ii+1} + \sum_{k=1}^{j-1}\epsilon|h_k|^2\rho_k + \sum_{k=j+1}^{i}|h_k|^2\rho_k}\right]df\right] \tag{27}$$

$$C_{ij} = \int_{B_{ii+1}} E\left[\log_2\left[B_{ii+1} + \sum_{k=1}^{j-1}\epsilon|h_k|^2\rho_k + \sum_{k=j}^{i}|h_k|^2\rho_k\right]\right]df - \int_{B_{ii+1}} E\left[\log_2\left[B_{ii+1} + \sum_{k=1}^{j-1}\epsilon|h_k|^2\rho_k + \sum_{k=j+1}^{i}|h_k|^2\rho_k\right]\right]df \tag{28}$$

Let assume X, Y are random variables given by, $X \triangleq \sum_{k=1}^{j-1}\epsilon|h_k|^2\rho_k + \sum_{k=j}^{i}|h_k|^2\rho_k$, $Y \triangleq \sum_{k=1}^{j-1}\epsilon|h_k|^2\rho_k + \sum_{k=j+1}^{i}|h_k|^2\rho_k$, respectively. The probability density functions (pdf) of X and Y are given by [51],

$$f_X(x) = \left(\prod_{m=1}^{i}\beta_m\right)\sum_{n=1}^{i}\frac{e^{-\beta_m x}}{\prod_{\substack{p=1\\p\neq n}}^{i}(\beta_p - \beta_n)} \tag{29}$$

$$f_Y(y) = \left(\prod_{\substack{m=1\\m\neq j}}^{i}\beta_m\right)\sum_{\substack{n=1\\n\neq j}}^{i}\frac{e^{-\beta_m y}}{\prod_{\substack{p=1\\p\neq n,j}}^{i}(\beta_p - \beta_n)} \tag{30}$$

where, $\beta_m = \epsilon\beta'_m, m \in [1, j-1]$ and $\beta_m = \beta'_m, m \in [j, i]$. By substituting the X, Y and their pdfs' in (28), we get,

$$C_{ij} = \int_{B_{ii+1}}\int_{0}^{\infty}\log_2\left[B_{ii+1} + X\right]f_X(x)\ dx\ df - \int_{B_{ii+1}}\int_{0}^{\infty}\log_2\left[B_{ii+1} + Y\right]f_Y(y)\ dy\ df \tag{31}$$

By applying the $\int_0^\infty e^{-\mu x}\ln(\varphi + x)dx = \frac{1}{\mu}[\ln\varphi - e^{\mu\beta}Ei(-\beta\mu)]$, where $Ei(.)$ denotes exponential integral function, the mathematical expression for the data rates achieved by node S_j in the B_{ii+1} bandwidth is given by,

$$C_{ij} = \int_{B_{ii+1}}\left(\prod_{m=1}^{i}\beta_m\right)\left(\sum_{n=1}^{i}\frac{1}{B_{ii+1}}(\ln(B_{ii+1}) - e^{(\beta_n B_{ii+1})}Ei(-B_{ii+1}\beta_n)\right)df - \int_{B_{ii+1}}\left(\prod_{\substack{m=1,\\m\neq j}}^{i}\beta_m\right)\left(\sum_{\substack{n=1,\\n\neq j}}^{i}\frac{1}{B_{ii+1}}\left(\ln(B_{ii+1}) - e^{(\beta_n B_{ii+1})}Ei(-B_{ii+1}\beta_n)\right)\right)df \tag{32}$$

■

APPENDIX B
DERIVATION OF THEOREM 2

Proof: The probability of success in the proposed ALOHA-NOMA scheme is the sum of probability of success in which r and less than r number of nodes transmitting the data packets simultaneously. Mathematically, $P_s = \sum_{j=1}^{r}P_{s_j}$, where P_{s_j} represents the probability of success in which j number of nodes transmitting the data packets. The expression for P_{s_j} is given by,

$$P_{s_j} = \binom{r}{j}\frac{\binom{\frac{N}{r}}{1}^j}{\binom{N}{j}}\frac{((N-1)\lambda T)^j e^{-((N-1)\lambda T)}}{j!}, \tag{33}$$

where, $\frac{\binom{\frac{N}{r}}{1}^j}{\binom{N}{j}}$ represents the probability in which the no more than one node is transmitting from the same region, and $\binom{r}{j}$ gives the number of such different combinations. By substituting the P_{s_j} in P_s, the probability of success

in ALOHA-NOMA is obtained as the equation given in (15). ■

APPENDIX C
DERIVATION OF THEOREM 3

Proof: Energy consumed per bit in the proposed ALOHA-NOMA scheme is the sum of energy consumed in the r and less than r number of nodes transmitting the data packets simultaneously. Mathematically, $E = \sum_{j=1}^{r} E_j$, where E_j represents the average energy consumed per bit in which j number of nodes transmitting the data packets. The expression for E_j is given by, $E_j = \frac{(P_{tr}+\frac{P_{sleep}}{\lambda})}{P_{s_j}\times C_j}$. By substituting the E_j in E, the energy consumed per bit in ALOHA-NOMA is obtained as the equation given in (19). ■

APPENDIX D
DERIVATION OF THEOREM 4

Proof: We consider $a = (N-1)T$. MAC layer utilization factor maximizing channel attempt rate (λ^*) is obtained by differentiating MAC layer utilization factor with respect to attempt rate and equating to zero. Accordingly, we obtain

$$\frac{dU(\lambda)}{d\lambda} = \frac{d}{d\lambda}\left(\frac{T}{T+\frac{1}{\lambda}}\sum_{j=1}^{r}\binom{r}{j}\frac{\left(\binom{\frac{N}{r}}{1}\right)^j}{\binom{N}{j}}\frac{(a\lambda)^j e^{-(a\lambda)}}{(j)!}\right) = 0$$

$$\frac{dU(\lambda)}{d\lambda} = \sum_{j=1}^{r}\frac{d}{d\lambda}\left(\frac{T}{T+\frac{1}{\lambda}}\binom{r}{j}\frac{\left(\binom{\frac{N}{r}}{1}\right)^j}{\binom{N}{j}}\frac{(a\lambda)^j e^{-(a\lambda)}}{(j)!}\right) = 0 \tag{34}$$

Accordingly, after performing differentiation with respect to λ, we obtain

$$\frac{dU(\lambda)}{d\lambda} = \frac{T(\lambda T+1)-\lambda TT}{(\lambda T+1)^2}\sum_{j=1}^{r}\binom{r}{j}\frac{\left(\binom{\frac{N}{r}}{1}\right)^j}{\binom{N}{j}}\frac{(a\lambda)^j e^{-(a\lambda)}}{j!} + \frac{\lambda T}{(\lambda T+1)}\sum_{j=1}^{r}\binom{r}{j}\frac{\left(\binom{\frac{N}{r}}{1}\right)^j}{\binom{N}{j}}\frac{j}{\lambda}\frac{(a\lambda)^j e^{-(a\lambda)}}{j!} - \frac{\lambda T}{(\lambda T+1)}\sum_{j=1}^{r}\binom{r}{j}\frac{\left(\binom{\frac{N}{r}}{1}\right)^j}{\binom{N}{j}}\frac{a(a\lambda)^j e^{-(a\lambda)}}{j!} = 0 \tag{35}$$

$$\frac{dU(\lambda)}{d\lambda} = \frac{T}{(\lambda T+1)^2}\sum_{j=1}^{r}\binom{r}{j}\frac{\left(\binom{\frac{N}{r}}{1}\right)^j}{\binom{N}{j}}\frac{(a\lambda)^j e^{-(a\lambda)}}{j!} + \frac{\lambda T}{(\lambda T+1)}\sum_{j=1}^{r}\binom{r}{j}\frac{\left(\binom{\frac{N}{r}}{1}\right)^j}{\binom{N}{j}}\frac{j}{\lambda}\frac{(a\lambda)^j e^{-(a\lambda)}}{j!} - \frac{\lambda T}{(\lambda T+1)}\sum_{j=1}^{r}\binom{r}{j}\frac{\left(\binom{\frac{N}{r}}{1}\right)^j}{\binom{N}{j}}\frac{a(a\lambda)^j e^{-(a\lambda)}}{j!} = 0 \tag{36}$$

Simplifying (36), we get characteristic function as given by,

$$\sum_{j=1}^{r}\left[\frac{T}{(\lambda T+1)^2}+\frac{\lambda T}{(\lambda T+1)}\left[\frac{j}{\lambda}-a\right]\right]\binom{r}{j}\frac{\left(\binom{\frac{N}{r}}{1}\right)^j}{\binom{N}{j}}\frac{(a\lambda)^j e^{-(a\lambda)}}{(j)!} = 0 \tag{37}$$

■

REFERENCES

[1] W. Tian et al., "A centralized control-based clustering scheme for energy efficiency in underwater acoustic sensor networks," *IEEE Trans. Green Commun. Netw.*, vol. 7, no. 2, pp. 668–679, Jun. 2023.

[2] X. Zhong, F. Chen, Z. Jiang, F. Ji, M. Tao, R. Xie, and K. Ding, "Performance analysis of underwater acoustic sensor networks with buffer constraint," *IEEE Internet Things J.*, vol. 11, no. 6, pp. 9392–9404, Mar. 2024.

[3] N. Adam, M. Ali, F. Naeem, A. S. Ghazy, and G. Kaddoum, "State-of-the-art security schemes for the Internet of Underwater Things: A holistic survey," *IEEE Open J. Commun. Soc.*, vol. 5, pp. 6561–6592, 2024.

[4] R. Guida, E. Demirors, N. Dave, and T. Melodia, "Underwater ultrasonic wireless power transfer: A battery-less platform for the Internet of Underwater Things," *IEEE Trans. Mobile Comput.*, vol. 21, no. 5, pp. 1861–1873, May 2022.

[5] J. Pei, W. Liu, L. Wang, C. Liu, A. K. Bashir, and Y. Wang, "Fed-IoUT: Opportunities and challenges of federated learning in the Internet of Underwater Things," *IEEE Internet Things Mag.*, vol. 6, no. 1, pp. 108–112, Mar. 2023.

[6] J. Bolboli, M. Salman, R. Prasad Naik, and W.-Y. Chung, "Design and performance evaluation of a relay-assisted hybrid lora/optical wireless communication system for IoUT," *IEEE Open J. Commun. Soc.*, vol. 5, pp. 4046–4060, 2024.

[7] Y. Song, "Underwater acoustic sensor networks with cost efficiency for Internet of Underwater Things," *IEEE Trans. Ind. Electron.*, vol. 68, no. 2, pp. 1707–1716, Feb. 2021.

[8] L. Wang, C. Lin, K. Chen, and Y. Zhang, "A learning-based aloha protocol for underwater acoustic sensor networks," in *Proc. 13th ACM Int. Conf. Underwater Netw. Syst.*, 2018, p. 15. [Online]. Available: https://doi.org/10.1145/3291940.3291942

[9] M. Cicioğlu and A. Çalhan, "Performance analysis of cross-layer design for Internet of Underwater Things," *IEEE Sensors J.*, vol. 22, no. 15, pp. 15429–15434, Aug. 2022.

[10] J. Jiang, W. Tian, G. Han, and F. Zhang, "A medium access control protocol based on parity group-graph coloring for underwater AUV-aided data collection," *IEEE Internet Things J.*, vol. 11, no. 4, pp. 5967–5979, Feb. 2024.

[11] J. Ahn, A. Syed, B. Krishnamachari, and J. Heidemann, "Design and analysis of a propagation delay tolerant aloha protocol for underwater networks," *Ad Hoc Netw.*, vol. 9, no. 5, pp. 752–766, 2011. [Online]. Available: http://www.sciencedirect.com/science/article/pii/S1570870510001472

[12] P. Mandal, S. De, and S. S. Chakraborty, "A receiver synchronized slotted aloha for underwater wireless networks with imprecise propagation delay information," *Ad Hoc Netw.*, vol. 11, no. 4, pp. 1443–1455, 2013. [Online]. Available: http://www.sciencedirect.com/science/article/pii/S1570870511000412

[13] Y. Zhu, Z. Peng, J.-H. Cui, and H. Chen, "Toward practical MAC design for underwater acoustic networks," *IEEE Trans. Mobile Comput.*, vol. 14, no. 4, pp. 872–886, Apr. 2015.

[14] M. Koseoglu, E. Karasan, and L. Chen, "Cross-layer energy minimization for underwater aloha networks," *IEEE Syst. J.*, vol. 11, no. 2, pp. 551–561, Jun. 2017.

[15] K. S. Geethu and A. V. Babu, "Energy optimal channel attempt rate and packet size for aloha based underwater acoustic sensor networks," *Telecommun. Syst.*, vol. 65, no. 3, pp. 429–442, Jul. 2017. [Online]. Available: https://doi.org/10.1007/s11235-016-0246-3

[16] X. Zhong, Z. Jiang, F. Chen, X. Zhu, and M. Tao, "Throughput analysis on slotted underwater acoustic sensor networks with guard time," *IEEE Sensors J.*, vol. 23, no. 3, pp. 3313–3320, Feb. 2023.
[17] Y. Zhou, K. Chen, J. He, and H. Guan, "Enhanced slotted aloha protocols for underwater sensor networks with large propagation delay," in *Proc. IEEE 73rd Veh. Technol. Conf. (VTC Spring)*, May 2011, pp. 1–5.
[18] H. Yu, N. Yao, S. Cai, and Q. Han, "Analyzing the performance of aloha in string multi-hop underwater acoustic sensor networks," *EURASIP J. Wireless Commun. Netw.*, vol. 2013, no. 1, p. 65, Mar. 2013. [Online]. Available: https://doi.org/10.1186/1687-1499-2013-65
[19] Y. M. Aval, Y. Han, A. Tu, S. Basagni, M. Stojanovic, and Y. Fei, "Testbed-based performance evaluation of handshake-free mac protocols for underwater acoustic sensor networks," in *Proc. OCEANS MTS/IEEE Monterey*, 2016, pp. 1–7.
[20] N. Chirdchoo, W.. Soh, and K. C. Chua, "Aloha-based MAC protocols with collision avoidance for underwater acoustic networks," in *Proc. IEEE INFOCOM 26th IEEE Int. Conf. Comput. Commun.*, 2007, pp. 2271–2275.
[21] Y. Zhou, H. Yang, Y.-H. Hu, and S.-Y. Kung, "Cross-layer network lifetime maximization in underwater wireless sensor networks," *IEEE Syst. J.*, vol. 14, no. 1, pp. 220–231, Mar. 2020.
[22] M. Elkourdi, A. Mazin, and R. D. Gitlin, "Slotted aloha-noma with MIMO beamforming for massive M2M communication in IoT networks," in *Proc. IEEE 88th Veh. Technol. Conf. (VTC-Fall)*, 2018, pp. 1–5.
[23] J. Jiang, Q. Yan, G. Han, and H. Wang, "An opportunistic routing based on directional transmission in the Internet of Underwater Things," *IEEE Internet Things J.*, vol. 10, no. 18, pp. 16392–16403, Sep. 2023.
[24] J. Guo, S. Song, J. Liu, H. Chen, J.-H. Cui, and G. Han, "A hybrid NOMA-based MAC protocol for underwater acoustic networks," *IEEE/ACM Trans. Netw.*, vol. 32, no. 2, pp. 1187–1200, Apr. 2024.
[25] N. Abramson, "The ALOHA system-another alternative for computer communications," in *Proc. Int. Workshop Managing Requirements Knowl.*, Nov. 1970, p. 281. [Online]. Available: https://doi.ieeecomputersociety.org/10.1109/AFIPS.1970.138
[26] Y. Sun, W. Ge, Y. Li, and J. Yin, "Cross-layer protocol based on directional reception in underwater acoustic wireless sensor networks," *J. Marine Sci. Eng.*, vol. 11, no. 3, p. 666, 2023. [Online]. Available: https://www.mdpi.com/2077-1312/11/3/666
[27] M. Jain, S. Soni, N. Sharma, and D. Rawal, "Performance analysis at far and near user in NOMA based system in presence of sic error," *AEU Int. J. Electron. Commun.*, vol. 114, 2020, Art. no. 152993.
[28] Y. Zhang, Z. Yang, Y. Feng, and S. Yan, "Performance analysis of cooperative relaying systems with power-domain non-orthogonal multiple access," *IEEE Access*, vol. 6, pp. 39839–39848, 2018.
[29] Y. Liu, Z. Qin, M. Elkashlan, Z. Ding, A. Nallanathan, and L. Hanzo, "Nonorthogonal multiple access for 5G and beyond," *Proc. IEEE*, vol. 105, no. 12, pp. 2347–2381, Dec. 2017.
[30] J. Kim and I. Lee, "Capacity analysis of cooperative relaying systems using non-orthogonal multiple access," *IEEE Commun. Lett.*, vol. 19, no. 11, pp. 1949–1952, Nov. 2015.
[31] S. Soni, R. Makkar, D. Rawal, and N. Sharma, "Performance of selective DF-based multiple relayed noma system with imperfect CSI and SIC errors," *IEEE Trans. Green Commun. Netw.*, vol. 8, no. 1, pp. 79–89, Mar. 2024.
[32] W. Fan, P. Fan, and Z. Ding, "On the throughput of NOMA-ALOHA in massive IoT with sparse active users," *IEEE Wireless Commun. Lett.*, vol. 13, no. 3, pp. 582–586, Mar. 2024.
[33] S. R. C. Magalhães, S. Bayhan, and G. Heijenk, "Impact of power consumption models on the energy efficiency of downlink noma systems," *IEEE Trans. Green Commun. Netw.*, vol. 7, no. 4, pp. 1739–1753, Dec. 2023.
[34] H. Nooh, S. Won, S. X. Ng, M. F. Sohail, M. Kim, and M. El-Hajjar, "Optimal user pairing strategy for minimum power utilization in downlink non-orthogonal multiple access systems," *IEEE Open J. Commun. Soc.*, vol. 5, pp. 4125–4137, 2024.
[35] A. Salem, X. Tong, A. Li, and C. Masouros, "Noma made practical: Removing the receive sic processing through interference exploitation," *IEEE Open J. Commun. Soc.*, vol. 5, pp. 2723–2734, 2024.
[36] J. Cheon and H.-S. Cho, "Power allocation scheme for non-orthogonal multiple access in underwater acoustic communications," *Sensors*, vol. 17, no. 11, p. 2465, 2017.
[37] M. J. Bocus, D. Agrafiotis, and A. Doufexi, "Non-orthogonal multiple access (NOMA) for underwater acoustic communication," in *Proc. IEEE 88th Veh. Technol. Conf. (VTC-Fall)*, 2018, pp. 1–5.
[38] M. Jain, N. Sharma, A. Gupta, D. Rawal, and P. Garg, "Performance analysis of NOMA assisted underwater visible light communication system," *IEEE Wireless Commun. Lett.*, vol. 9, no. 8, pp. 1291–1294, Aug. 2020.
[39] V. Goutham and V. P. Harigovindan, "Noma based cooperative relaying strategy for underwater acoustic sensor networks under imperfect SIC and imperfect CSI: A comprehensive analysis," *IEEE Access*, vol. 9, pp. 32857–32872, 2021.
[40] V. Goutham and V. Harigovindan, "Full-duplex cooperative relaying with noma for the performance enhancement of underwater acoustic sensor networks," *Eng. Sci. Technol. Int. J.*, vol. 24, no. 6, pp. 1396–1407, 2021. [Online]. Available: https://www.sciencedirect.com/science/article/pii/S2215098621000641
[41] E. A. Makled, A. Yadav, O. A. Dobre, and R. D. Haynes, "Hierarchical full-duplex underwater acoustic network: A NOMA approach," in *Proc. OCEANS MTS/IEEE Charleston*, 2018, pp. 1–6.
[42] A. A. Tegos, S. A. Tegos, D. Tyrovolas, P. D. Diamantoulakis, P. Sarigiannidis, and G. K. Karagiannidis, "Breaking orthogonality in uplink with randomly deployed sources," *IEEE Open J. Commun. Soc.*, vol. 5, pp. 566–582, 2024.
[43] M. C. Domingo and R. Prior, "Energy analysis of routing protocols for underwater wireless sensor networks," *Comput. Commun.*, vol. 31, no. 6, pp. 1227–1238, 2008. [Online]. Available: http://www.sciencedirect.com/science/article/pii/S0140366407004689
[44] R. J. Urick, *Principles Of Underwater Sound*.3rd ed. Los Altos, CA, USA: Peninsula Publishing, 1983.
[45] H. U. Yildiz, V. C. Gungor, and B. Tavli, "Packet size optimization for lifetime maximization in underwater acoustic sensor networks," *IEEE Trans. Ind. Informat.*, vol. 15, no. 2, pp. 719–729, Feb. 2019.
[46] R. E. Francois and G. R. Garrison, "Sound absorption based on ocean measurements: Part I: Pure water and magnesium sulfate contributions," *J. Acoust. Soc. America*, vol. 72, no. 3, pp. 896–907, 1982. [Online]. Available: https://doi.org/10.1121/1.388170
[47] R. E. Francois and G. R. Garrison, "Sound absorption based on ocean measurements. part II: Boric acid contribution and equation for total absorption," *J. Acoust. Soc. America*, vol. 72, no. 6, pp. 1879–1890, 1982. [Online]. Available: https://doi.org/10.1121/1.388673
[48] K. V. Mackenzie, "Nine-term equation for sound speed in the oceans," *J. Acoust. Soc. America*, vol. 70, no. 3, pp. 807–812, 1981.
[49] M. Stojanovic, "On the relationship between capacity and distance in an underwater acoustic communication channel," in *Proc. 1st ACM Int. Workshop Underwater Netw.*, 2006, pp. 41–47. [Online]. Available: http://doi.acm.org/10.1145/1161039.1161049
[50] Y. Li, Y. Zhang, H. Zhou, and T. Jiang, "To relay or not to relay: Open distance and optimal deployment for linear underwater acoustic networks," *IEEE Trans. Commun.*, vol. 66, no. 9, pp. 3797–3808, Sep. 2018.
[51] E. Levy, "On the density for sums of independent exponential, Erlang and gamma variates," *Stat. Papers*, vol. 63, no. 3, pp. 693–721, 2022.

VEERAPU GOUTHAM (Member, IEEE) received the Undergraduate degree in electronics and communication engineering from Sri Krishnadevaraya University, Anantapur, India, and the Postgraduate degree in digital communications from the National Institute of Technology Bhopal, India, and the Ph.D. degree in wireless communications from the National Institute of Technology Puducherry, in 2022. He is currently serving as an Assistant Professor Senior Grade 1 with the Department of Communication Engineering, School of Electronics Engineering, Vellore Institute of Technology, Vellore, India. He has more than 20 international publications and one granted patent to his credit. His research interests are in the areas of non-orthogonal multiple access, 5G and beyond networks, intelligent reflecting surfaces, wireless communications, and underwater acoustic sensor networks.

V. P. HARIGOVINDAN (Senior Member, IEEE) received the Bachelor of Technology degree in electronics and communication engineering from the University of Calicut, the Master of Technology degree in digital electronics and communication systems from Visvesvaraya Technological University (with first rank), and the Ph.D. degree from the National Institute of Technology Calicut, in 2013. He is currently a Professor with the Department of Electronics and Communication Engineering, and the Dean (Planning and Development) of the National Institute of Technology Puducherry (under the Ministry of Education, Government of India). He has more than 75 international publications to his credit. He served as the Principal Investigator for three funded projects, each from the Department of Science and Technology, Government of India, Science and Engineering Research Board, and Microsoft AI for Earth. He is currently serving as the PI of a project funded by DST–Science for Equity, Empowerment, and Development, Government of India. He has seven patents granted to his credit. His research interests include wireless networks, artificial intelligence, Internet of things, and wireless communications.

MIRIYALA MAHESH (Member, IEEE) received the B.Tech. degree in electronics and communication engineering from Jawaharlal Nehru Technological University Hyderabad, the M.Tech. degree in embedded systems from the JNTUA College of Engineering Anantapuramu, Anantapur, and the Ph.D. degree in electronics and communication engineering from the National Institute of Technology Puducherry, Karaikal. He has published several papers in peer-reviewed journals, such as IEEE COMMUNICATIONS LETTERS, IEEE NETWORKING LETTERS, and *Computer communications*. He has also been granted three patents for his work on IEEE 802.11ah-based Wireless Local Area Networks. His fields of research interest are embedded systems, wireless communications, Internet of Things, 5G networks, NOMA, and IEEE 802.11ah.

DUSHANTHA NALIN K. JAYAKODY (Senior Member, IEEE) received the M.Sc. degree in electronics and communications engineering from Eastern Mediterranean University, Türkiye, and the Ph.D. degree in electronics and communications engineering from University College Dublin, Ireland, in 2014. He is a currently a Professor with the Lusófona University, Portugal, and the Faculty of Engineering, Sri Lanka Institute of Information Technology, Sri Lanka. He has held Visiting and/or Sabbatical positions with the Center for Telecommunications Research, University of Sydney, Australia, in 2015, and also with Texas A&M University, USA, in 2018. He was a Visiting Professor with the University of Jyväskylä, Finland, in 2019 and 2022, under the framework of the Academy of Finland. Additionally, he served as a Visiting Professor with the University of Juiz de Fora, Brazil, in 2019. From 2019 to 2022 and from 2024 to 2026, he has served as an SPARC Professor with the Department of Electronics and Communication Engineering, National Institute of Technology, Tiruchirappalli, India, under the framework of the Ministry of Human Resource Development, India. From 2014 to 2016, he was a Postdoctoral Research Fellow with the University of Tartu, Estonia, and the University of Bergen, Norway. From 2016 to 2021, he was a Professor with the School of Computer Science and Robotics, National Research Tomsk Polytechnic University, Russia. From 2019 to 2021, he served as the Dean of the School of Postgraduate Studies and Research and the Director of Postgraduate, Research, and Impact, Sri Lanka Technological Campus, Sri Lanka, from 2021 to 2022. He was also associated with the Department of Engineering and Computer Science, Autónoma TechLab, Universidade Autónoma de Lisboa, Portugal, from 2021 to 2022. He has supervised over ten Ph.D. students, numerous master's students, more than 50 undergraduate students, and five postdoctoral researchers. Throughout his career, he has secured nearly 6 million in research funding from various international grant agencies and published over 230 peer-reviewed journal articles, conference papers, and books. He has received several prestigious awards, including the Best Paper Award from the IEEE ICCMIT 2017, the ETIC 2019, the ICARC 2024, the ICAC 2024, and the IRC 2023. In July 2019, he was honored with the Education Leadership Award from the World Academic Congress. In 2017 and 2018, he received the Outstanding Faculty Award from National Research Tomsk Polytechnic University, Russia. He was also received various awards at University level from his previous employers. In 2021, he received the Sri Lankan Presidential Award for his outstanding research performance, among many other awards and recognitions. He was ranked among the top 2% scientists in the world in 2021, 2022, and 2023, according to the Stanford-Elsevier list. Additionally, he was recognized as the Distinguished Researcher in Wireless Communications, Chennai, India, in 2019. He is a Fellow of IET.